AIAA 96-2493

APPLICATION OF NONLINEAR INDICIAL MODELING TO THE PREDICTION OF A DYNAMICALLY STALLING WING

Patrick H. Reisenthel[1]
Nielsen Engineering & Research, Inc.
Mountain View, CA

ABSTRACT

A nonlinear indicial prediction model was developed to predict the time-dependent unsteady aerodynamic loads associated with flight maneuvers at high angles of attack and high pitch rates. This model is based on nonlinear indicial theory and on efficient parameterization of the indicial and critical-state responses. The parameterization is based only on "local" information, such as instantaneous angle of attack and pitch rate. The present paper describes the application of this nonlinear indicial model to the prediction of the unsteady aerodynamic loads associated with a rectangular wing undergoing dynamic stall. The wing data used to validate the prediction is approximated by an artificial neural network which was trained to reproduce in detail the aerodynamic characteristics of the wing. It is shown that only a finite number of indicial and critical-state responses is necessary in order to accurately construct the flow responses for novel maneuvers.

NOMENCLATURE

Symbols and abbreviations

B	Box function
c	Wing chord
C_d	Sectional drag coefficient
C_D	Drag coefficient
C_L	Lift coefficient
C_l	Sectional lift coefficient
C_m	Sectional pitching moment coefficient
C_n	Sectional normal force coefficient
C_p	Pressure coefficient
C_t	Sectional tangential force coefficient
CSR	Critical-state Response
H	Heaviside step function
k	Reduced frequency ($k \equiv \omega c/2U_\infty$)
q	Pitch rate
QS	Quasi-static
t	Time
t^*	Time at which the indicial step is applied
U_∞	Freestream velocity
α	Angle of attack
α^+	Nondimensional pitch rate $\left(\alpha^+ \equiv \frac{\dot{\alpha} c}{U_\infty}\right)$
τ	Auxiliary time variable
τ_c	Time at which critical state is crossed
Δt	Sampling period (nondimensionalized by c and U_∞)
ξ	Parameter denoting dependence on prior motion history
ω	Angular frequency

Subscripts

CS	Critical State
dyn	Dynamic
max	Maximum
min	Minimum
qs	Quasi-static
s	Stall
∞	Time-asymptotic value (except for U_∞)

Superscripts

CS	Critical State
s	Stall
•	Derivative with respect to time
••	Second derivative with respect to time
~	Indicial function
*	Evaluation at the time of the indicial step

[1] Chief Scientist, Member AIAA

1. INTRODUCTION

In recent years, it has been possible to integrate the flight-dynamics equations fairly efficiently using linearized aerodynamics which are occasionally supplemented with ad hoc methods (i.e., semiempirical simulations or wind tunnel data) to include nonlinear unsteady aerodynamic effects. With the expanded flight envelopes being considered for future maneuvering aircraft, it has become increasingly important to be able to model and predict nonlinear, unsteady aerodynamics. This includes the prediction of the aerodynamic response in the presence of flow separation, shock movement, and vortex bursting, among other phenomena, at high angles of attack and/or high angular rates. Existing flow prediction methods are either too expensive or lack the proper fidelity to represent the physics of the aerodynamic flow. A consequence of the poor modeling fidelity is a greater design uncertainty, lack of performance, and, possibly, expensive redesigns and retrofits of existing fleet vehicles, such as the F−18.

Future fighter aircraft will be required to perform controlled maneuvers well beyond traditional aircraft limits, for example, pitch up and flight at high angles of attack, rapid point-to-shoot, and other close-in combat maneuvers. To perform these ultrafast multi-axis motions, future tactical aircraft and missiles will pioneer the use of innovative technologies such as thrust vectoring control. To produce the best aircraft for these extreme flight conditions, it is necessary to combine successfully several disciplines in the design phase of the aircraft: flight mechanics, unsteady aerodynamics, flexible structural modeling, and control system simulation/design.

These advanced maneuvers demand the use of aerodynamic methods capable of predicting characteristics of the nonlinear post-stall regime for multiaxis motions at extremely high rates. At present, the only methods of this scope are Navier-Stokes methods. However, their use in flight simulations remains impractical at this time. Nonlinear indicial theory has the potential to circumvent some of the present difficulties, while providing a fidelity to the flow physics of which other methods appear incapable.

2. OBJECTIVE AND APPROACH

In order to predict the dynamics of maneuvering aircraft or missiles at high rotational rates and high angles of attack, it is essential to accurately and efficiently model the nonlinearities associated with post-stall aerodynamics, including bifurcations and hysteresis. Nonlinear indicial theory offers a viable alternative which can fulfill the need for the efficient and accurate modeling of nonlinear "plant" characteristics. The knowledge of these characteristics is a prerequisite for structural response feedback techniques and control system configuration design. The goal of this effort is to provide an unsteady aerodynamic model based on nonlinear indicial response theory. An important note concerning the application of nonlinear indicial theory is that the indicial functions (responses) can be obtained from numerical computations, experimental tests, or by analytic means, whichever is appropriate or available.

This paper is the second of two papers based on the present study. The validation of the nonlinear indicial approach for predicting unsteady aerodynamic loads at high α was performed on two distinct models for the unsteady aerodynamic responses. The first model (and the topic of the first paper, Ref. 1) is a two-parameter delay differential equation model approximating the pitch plane high angle-of-attack maneuvering of a fighter aircraft (full scale). The second model (and the topic of this second paper) is an artificial neural network which was trained to reproduce the high angle-of-attack aerodynamic characteristics of a pitching rectangular wing (wind tunnel test, Ref. 2).

3. BACKGROUND

Much of the technical background for this work can be found in Ref. 1. However, a brief description of linear and nonlinear theory is given below for completeness.

3.1. Linear Indicial Theory

The indicial approach is based on the concept that a characteristic flow variable $f(\bar{x},t)$, which describes the state of the flow, can be linearized with respect to its boundary condition (or forcing function), ϵ(t), if the variation of $f(\bar{x},t)$ is a smooth function of ϵ(t). This allows the representation of $f(\bar{x},t)$ in a Taylor

series about some value of $\epsilon = \epsilon_0$; thus

$$f(\bar{x},t) = f(\bar{x},0) + \Delta\varepsilon \left.\frac{\partial f}{\partial \varepsilon}\right|_{\varepsilon=\varepsilon_0} + \cdots$$

If $f(\bar{x},0)$ is zero (a zero initial condition), then an approximate solution is

$$f(\bar{x},t) = \Delta\varepsilon \left.\frac{\partial f}{\partial \varepsilon}\right|_{\varepsilon=\varepsilon_0} \qquad (1)$$

Equation (1) is an approximation which becomes more accurate as $\Delta\varepsilon \to 0$. Also, Eq. (1) is exact if $f(\bar{x},t)$ is a linear function of ϵ(t). If the response $\partial f/\partial \varepsilon$ depends only on the elapsed time from the perturbation $\Delta\epsilon$ (a linear time invariant response) then it may be shown (Ref. 3) that the formal solution for $f(\bar{x},t)$ is

$$f(\bar{x},t) = \tilde{f}(\bar{x},t)\,\varepsilon(0) + \int_0^t \frac{d\varepsilon}{d\tau}\,\tilde{f}(\bar{x},t-\tau)\,d\tau \qquad (2)$$

where $\tilde{f}(\bar{x},t) = \left.\dfrac{\partial f}{\partial \varepsilon}\right|_{\varepsilon=\varepsilon_0}$.

Hence, if the forcing function (i.e., the boundary condition ϵ) is known and if $\tilde{f}$ is known from some computation or experimental determination, then Eq. (2) gives the value of $f(\bar{x},t)$ for any schedule of boundary conditions ϵ(t) without the need to compute $\tilde{f}$ from first principles. This has the effect of reducing computational costs considerably. Equation (2) is a semi-analytic relation between $f(\bar{x},t)$ and its boundary condition or forcing function ϵ(t). The symbol $\bar{x}$ represents a set of independent variables x_i such as spatial coordinates. For simplicity, if these variables do not depend on time, they (x_i) are omitted in subsequent discussions.

As a general rule, linear indicial theory is valid away from bifurcations such as changes in flow topology, and provided that the perturbation displacements are small. Linear indicial theory has been validated in numerous examples ranging from unsteady transonic flow around airfoils (Ref. 4) and missile bodies (Ref. 5) to separated flow at low Reynolds numbers (Ref. 6). The nonlinear flow associated with finite amplitude perturbations ($\Delta\alpha \approx 5°$) relative to a reference pitching motion was also shown to be predicted accurately using Navier-Stokes indicial functions inferred in the Laplace domain (Ref. 7).

3.2. Nonlinear Indicial Theory

The basic idea behind the use of nonlinear indicial functions, as defined by Tobak et al. (Ref. 8) and Tobak and Chapman (Ref. 9) is that the linear formalism, Eq. (2), can be retained in the form of a generalized superposition integral, provided that the nonlinear indicial response $\tilde{f}$ is now taken to be a functional $\tilde{f}(\epsilon(\xi);t,\tau)$, where $\epsilon(\xi)$ denotes the dependence on the entire motion history:

$$f(t) = f(t;\varepsilon(0)) + \int_0^t \frac{d\varepsilon}{d\tau}\,\tilde{f}(\varepsilon(\xi);t,\tau)\,d\tau \qquad (3)$$

Equation (3) is, therefore, a generalization of the linear convolution model (Duhamel convolution integral), Eq. (2). It was formally shown that this formulation is equivalent to a nonlinear functional expansion of which the classical Volterra series is a subset. In the nonlinear indicial formulation, the nonlinear indicial function $\tilde{f}(\epsilon(\xi);t,\tau)$ is defined as the following Fréchet derivative:

$$\tilde{f}(\varepsilon(\xi);t,\tau) = \lim_{\Delta\varepsilon\to 0} \frac{\Delta f(t)}{\Delta\varepsilon}$$

$$= \lim_{\Delta\varepsilon\to 0} \left[\frac{f(\varepsilon(\xi) + H(\xi-\tau)\Delta\varepsilon) - f(\varepsilon(\xi))}{\Delta\varepsilon}\right]$$

where the step in boundary condition, $\Delta\epsilon$, is applied at time t = τ, and *H* designates the Heaviside step function.

Note from Eqs. (2) and (3) that the linear and nonlinear indicial function approaches differ fundamentally in two ways. First, the fact that $\tilde{f}(\epsilon(\xi);t,\tau)$ has a separate dependence on t and τ rather than on the elapsed time (t-τ) alone signifies that $\tilde{f}$ in the nonlinear formulation can now depend on the past history of the boundary conditions, i.e., "memory" effects are included in the kernel. Second, the functional dependency on $\epsilon(\xi)$ itself distinguishes the nonlinear indicial response from its linear counterpart. In practice, the quantity f of interest might typically be an integrated load (e.g., C_L) or generalized aerodynamic force (for flexible bodies), while the boundary condition ϵ might be an aeroelastic modal amplitude, or the angle of attack, α. In the latter case, the generalized superposition

integral, Eq. (3), may express the full dependence of C_L on prior motion, given any arbitrary schedule of $\alpha(t)$. This formalism is valid as long as f remains Fréchet-differentiable, a condition which is violated at bifurcation points.

In order to address this point, Tobak and Chapman (Ref. 9) modified the theory so as to include bifurcation points. These are identified as discrete points during the aircraft motion at which Fréchet differentiability is lost. This can be due to the loss of stability of a particular solution (or equilibrium state prior to the bifurcation) changing to a new equilibrium state which is stable. This discrete change to a new equilibrium at the critical (bifurcation) time τ_c is accommodated in the theory by splitting the generalized superposition integral as follows

$$f(t) = f(t;\varepsilon(0)) + \int_0^{\tau_c} \frac{d\varepsilon}{d\tau}\tilde{f}(\varepsilon(\xi);t,\tau)\,d\tau + \Delta f(t;\varepsilon(\tau_c)) + \int_{\tau_c}^{t} \frac{d\varepsilon}{d\tau}\tilde{f}(\varepsilon(\xi);t,\tau)\,d\tau$$

where

$$\Delta f(t;\varepsilon(\tau_c)) = f(\varepsilon(\xi);t,\tau_c+\delta\tau) - f(\varepsilon(\xi);t,\tau_c-\delta\tau)$$

is taken in the limit: $\delta\tau \to 0$. The term $\Delta f(t;\epsilon(\tau_c))$ represents the possibility of a discontinuous jump. Recent work (Ref. 10) at Wright Laboratory has shown, for example, that when a critical state of the flow is crossed, this gives rise to unusually long transients. These long transients are believed to be associated with the jump response, $\Delta f(t;\epsilon(\tau_c))$.

3.3. Nonlinear Indicial Prediction Model

The nonlinear indicial prediction model is based on nonlinear indicial theory and key simplifications thereof. Three technologies form the core of the model: (1) nonlinear indicial theory, (2) functional interpolation of parameterized responses, and (3) artificial intelligence-based techniques for partitioning the indicial function space. A basic description of the model is provided in Ref. 1. Key aspects related to the treatment of critical states are contained in Ref. 11.

4. METHOD

The development, testing, and validation of the nonlinear indicial prediction model require large amounts of unsteady aerodynamic data. Unsteady aerodynamic responses are necessary, both to generate the required indicial functions and critical-state responses, and to compare the indicial theoretical prediction to the data for arbitrary maneuvers.

It would be ideal to use unsteady aerodynamic responses inferred from experimental tests. At this time, however, many of the practical problems involved in extracting such information have not been resolved. An alternative is the use of Computational Fluid Dynamics (CFD), but this approach is expensive and impractical.

The approach taken in the present research has been to consider, instead, the use of efficient and, hopefully, reasonably accurate nonlinear models for the unsteady flow behavior. Specifically, two models were considered. The first model (referred to as the Goman-Khrabrov model) is an analytical model which approximates the flight test aerodynamic responses of a fighter aircraft undergoing "Cobra"-type maneuvers. The application of nonlinear indicial theory to this first example (i.e., the Goman-Khrabrov model) is the topic of Ref. 1. This first example is useful in understanding the foundations of the nonlinear indicial prediction model. However, it is a simple nonlinear model, in the sense that there are no crossings of critical states. The second model is an artificial neural network which was trained on wind tunnel data of a pitching rectangular wing undergoing dynamic stall (Ref. 2). This second application is an example of a highly nonlinear plant and includes at least one critical state (aerodynamic bifurcation), requiring special handling. The application of nonlinear indicial theory to the neural network example is the topic of the present paper.

To avoid any possible confusion, from here on the term "model" will be reserved for the nonlinear indicial prediction scheme referred to in Section 3.3. By contrast, the Goman-Khrabrov and neural network "models" (in the old terminology) will be referred to as "systems," since they approximate the behavior of real fluid systems (a pitching aircraft or a pitching wing). Accordingly, the output of these systems will be referred to as the "data," as opposed to the "prediction," which is the output of the indicial model.

The Goman-Khrabrov and neural network systems both exhibit complex nonlinear behavior. In each case, they are used (1) to generate the indicial and (if

required) critical-state-response data, and (2) to compare against the indicial theoretical prediction for novel maneuvers. The application of the indicial theoretical prediction method to the neural network system is described below.

5. APPLICATION OF THE METHOD TO THE NEURAL NETWORK SYSTEM

5.1. Description of the Neural Network System

The neural network was trained on wind tunnel data for a rectangular wing (NACA0015 profile, chord Reynolds number Re = 70,000) pitching about the 1/4 chord location. Several sets of data are available including pitch up from $\alpha = 0°$ to $\alpha = 60°$ (constant non-dimensional pitch rate $0.01 < \alpha^+ < 0.2$), pitch down (same bounds and pitch rates), and various harmonic wing motions with and without dynamic stall (overall range: $3° < \alpha < 25°$, $0.05 < k < 0.15$). For more detail, see Ref. 2.

The particular neural network program that is used in this study is the "pitch-up" neural network, which is treated as a "black box" substitute for the experiment. The pitch-up neural network predicts the sectional force coefficients C_l, C_d, C_n, C_t, and C_m in addition to the pressure coefficients at 15 locations on the upper surface. These predictions are made simultaneously at three span locations (0%, 37%, and 80% of the total wing span). The location of the pressure taps is shown in Fig. 1. The architecture of the neural network is schematically illustrated in Fig. 2. The neural network has an input layer with 47 entries (45 fed back C_p's, plus the instantaneous α and $d\alpha/dt$), two hidden layers, each with 32 neurodes, and 60 outputs (45 predicted C_p's and 15 force coefficients).

This neural network system was shown (Ref. 12) to replicate not only the constant pitch rate data it was trained on, but also to be able to predict the flow responses to "novel maneuvers" (both constant and variable pitch rates) with surprisingly high accuracy, provided that the physics of the flow are similar. For our purpose, the trained neural network can be considered as a "black box" prediction method for the time-dependent loads and pressure distributions. This black box prediction is an accurate representation of the flow within a reasonably wide parameter space, and it will be assumed that the flow responses predicted by the model are "as good" as if they were directly measured in wind tunnel tests. This is, of course, an imperfect assumption, and a more conservative viewpoint would be to consider the neural network simply as a nonlinear "plant" which "happens" to accurately model the flow responses under particular conditions. The practical advantages of using a neural network are substantial. In particular, the simulated unsteady aerodynamic loads resulting from many thousands of maneuvers can be generated at negligible cost. This allows modeling issues (for instance, the inclusion of critical states) to be resolved, while spending less time on the generation of flow responses, as would undoubtedly have been the case with either CFD or experiment.

A validation of the neural network was performed against the ensemble-averaged experimental data of Schreck and Faller (Refs. 2, 12, 13). The results of the validation study are described in Ref. 11. In particular, it was found that the comparison between the neural network and the experimental data tended to be more favorable at 0% span. Therefore, the remainder of this paper deals with the 0% span location.

5.2. Indicial Function Determination

The basic procedure for determining the indicial functions of the neural network system is the same as for the Goman-Khrabrov system of Ref. 1, namely, the straightforward application of the definition of the Fréchet derivative. Following the definition of the indicial response, two almost identical maneuvers $\alpha_1(t)$ and $\alpha_2(t)$ are carried out. The two maneuvers coincide for $t < \tau$. At $t = \tau$, the motion is stopped for the first maneuver ($\alpha_1(t) = \alpha_1(\tau)$, for $t \geq \tau$). The second maneuver is similarly stopped, except that the angle of attack is incremented by $\delta\alpha$ at time τ ($\alpha_2(t) = \alpha_2(\tau) + \delta\alpha$, for $t \geq \tau$). Let $C_{m,1}(t)$ and $C_{m,2}(t)$ denote the aerodynamic responses associated with $\alpha_1(t)$ and $\alpha_2(t)$, respectively. The indicial response is calculated as

$$\tilde{C}_m(t-\tau) \equiv \frac{\delta C_m(t-\tau)}{\delta\alpha} \approx \frac{C_{m_2}(t) - C_{m_1}(t)}{\delta\alpha} H(t-\tau)$$

This technique is referred to as the direct technique. Here, two points are worth noting. First, because the neural network output is a discrete time series at fixed non-dimensional time intervals (in this instance, $\Delta t = 0.12$), the "stepped" response required for the

determination of the indicial response is poorly approximated, resulting in a less accurate indicial function. The second area of difficulty is that, in order to approximate $\Delta\alpha(t) \propto H(t-\tau)$ *and* $\Delta(d\alpha/dt) \propto \delta(t-\tau)$ consistently in the limit $\Delta\alpha \to 0$, the possible values of t^* (the time at which the infinitesimal perturbation is applied) must be separated by multiples of the fixed sampling period, Δt. As in any numerical integration, the validity and accuracy of the globally constructed response depends on the indicial response being the leading order term in some Taylor series expansion valid about the local α. At a minimum, the radius of convergence of the series expansion should be larger than the integration step, $\Delta\alpha_{min} = \alpha^+ \Delta t$. Thus, provided that the indicial responses are smooth functions of α, an accurate numerical integration should be possible.

Early in the project, this was discovered not to be the case for the neural network. Rapid variations of the indicial functions were noted as a function of α. This is illustrated, for example, in Fig. 3 for the case of a nondimensional pitch rate $\alpha^+ = 0.04$. The indicial functions of the neural network are fairly regular (self-similar) only in the intervals $0° < \alpha < 15°$ and $25° < \alpha < 60°$. Furthermore, "catastrophic" nonlinearities are encountered near $\alpha = 16°$ to $17°$ angle of attack. Near these angles of attack, the indicial responses are characterized by unusually long transients, as well as reduced convergence properties with $\Delta\alpha \to 0$. Both of these characteristics can be seen in the example depicted in Fig. 4. (For reference, for all other indicial responses, convergence is obtained for $\Delta\alpha < 0.05°$).

The occurrence of extra long transients and the pathological sensitivity to the size of the indicial step both tend to suggest the proximity of a critical state. A further indication that this may be the case is the fact that the angle of attack range where this behavior is observed happens to be close to *static* stall (in contrast, dynamic stall, at $\alpha^+ = 0.04$, occurs around 23° angle of attack). The indicial function shown in Fig. 4 ($\alpha \approx 16.3°$) appears to be transitional between indicial functions (immediately prior to this angle-of-attack) where the quasi-static increment $dC_l/d\alpha$ is positive, and indicial functions (for slightly higher angles-of-attack) where $dC_l/d\alpha$ is negative. The implied discontinuity in $\partial(\delta C_l/\delta\alpha|_{\tau=\infty})/\partial\alpha$ (see Fig. 5) is, of course, another manifestation of static stall, and appears to support the critical-state hypothesis.

5.3. Critical State

In the absence of flow bifurcations, the nonlinear indicial theoretical prediction for (for example) C_l is given by the familiar generalized Duhamel convolution integral:

$$C_l(t) = C_l(0) + \int_0^t \left[\frac{\delta C_l(t-\tau)}{\delta\alpha}\right]_\tau \frac{d\alpha}{d\tau} d\tau$$

Use of this equation requires that C_l be Fréchet-differentiable, i.e., that

$$\frac{\delta C_l(\alpha(\xi);t,\tau)}{\delta\alpha} = \lim_{\Delta\alpha\to 0}\left[\frac{C_l(\alpha(\xi) + H(\xi-\tau)\Delta\alpha) - C_l(\alpha(\xi))}{\Delta\alpha}\right]$$

exists at all points in the interval [0,t]. At bifurcation points during the aircraft motion, Fréchet-differentiability is lost, by definition. This discrete change from one equilibrium state to another at the bifurcation time τ_c must be accounted for by splitting the generalized superposition integral as follows (see Ref. 9):

$$C_l(t) = C_l(0) + \int_0^{\tau_c-\epsilon}\left[\frac{\delta C_l(t-\tau)}{\delta\alpha}\right]_\tau \frac{d\alpha}{d\tau} d\tau + \Delta C_l^{CS}(t;\alpha(\tau_c)) + \int_{\tau_c+\epsilon}^t \left[\frac{\delta C_l(t-\tau)}{\delta\alpha}\right]_\tau \frac{d\alpha}{d\tau} d\tau$$

where

$$\Delta C_l^{CS}(t;\alpha(\tau_c)) = C_l(\alpha(\xi);t,\tau_c+\epsilon) - C_l(\alpha(\xi);t,\tau_c-\epsilon)$$

is taken in the limit: $\epsilon \to 0$.

One of the difficulties associated with the above formalism is the fact that it requires preemptive knowledge of the time instants τ_c at which bifurcations take place during the maneuver. In recent years, work at Wright Laboratory (see, e.g., Ref. 10) has shown that these bifurcations may be associated with the crossing of a "critical state." The crossing of a critical state during a maneuver is typically

associated with a change in flow topology (for example, the appearance/disappearance of separated flow regions, or the occurrence of vortex burst upstream of the trailing edge), and is characterized during unsteady maneuver by the existence of extra long transients. Most importantly, there is evidence that the existence of critical states may be predicted from quasi-static discontinuities, i.e., discontinuities of the static loads or their derivatives with respect to the state variable. The term ΔC_l^{CS} represents the possibility of a discontinuous jump. ΔC_l^{CS} will be referred to as the "critical-state response" (CSR, for short).

In order to circumvent the usual difficulties associated with a discrete time series (fixed $\Delta t = 0.12$) and, in particular, to pinpoint accurately the critical-state response, consider the quasi-static ramp $\alpha^+ = 0.0001$. For this low nondimensional pitch rate, each feedback iteration ("clock count") of the neural network corresponds to a step in angle of attack $\Delta\alpha \approx 0.00069°$ (as opposed to 0.275° at $\alpha^+ = 0.04$). The resulting quasi-static lift curve (Fig. 6) displays characteristics associated with precipitous stall, around $\alpha \approx 16.46°$. The existence of a nonzero critical-state response, ΔC_l^{CS}, was demonstrated by systematically "sliding" a window $[\tau_c-\epsilon,\tau_c+\epsilon]$ by the minimum increment $\Delta\tau_c=\epsilon$, using $\epsilon=\Delta t$. Using this method, the angle of attack at which the aerodynamic bifurcation occurs was determined to be $16.4043° \le \alpha \le 16.4050°$. Note that stall does not occur until $\alpha_s \approx 16.46°$, corresponding to as many as 80 clock counts of the neural network at $\alpha^+ = 0.0001$. This is, of course, a manifestation of the fact that the motion is not really quasi-steady, resulting in an already noticeable difference between the critical-state angle and the (dynamic) stall angle, i.e., in general:

$$\alpha_{CS} \neq \alpha_s$$

Figure 7 depicts the abrupt transition which takes place near the critical state. An extremely long transient (approximately 60 convective time scales) is observed prior to the jump.

A detailed analysis of the "anatomy" of the critical state is beyond the scope of the present paper. However, two figures are included to highlight some of the symptoms associated with the crossing of the critical state. Figure 8 depicts, on a linear scale, the narrow region where the time-asymptotic response is nonzero ($\Delta C_l^{CS}|_{\tau\to\infty} \approx -0.25$). Figure 9 depicts the gradual increase in the duration of the transient (defined as the elapsed time required for ΔC_l^{CS} to reach 95% of its time-asymptotic value) near the critical state. The singularity at α_{CS} is evident, and so are its precursor symptoms (the increase in transient length, from either side). Although the actual singularity is a well-defined point (see Fig. 8), the results of Ref. 13 support the notion that the critical state in the present system ought to be treated as a finite region, rather than a point.

Having determined the location of the critical state with good precision at $\alpha^+ = 0.0001$, it is relatively easy to locate the critical-state region for all pitch rates investigated ($0.0001 \le \alpha^+ \le 0.2$). The results (not shown here) suggest that α_{CS} is roughly constant as a function of pitch rate, which constitutes an important simplification, from a modeling perspective (see Section 5.6).

Figure 10 depicts the dynamic portion of the critical-state response at $\alpha^+ = 0.1$, defined as

$$\Delta C_{dyn}^{CS} = \Delta C^{CS}(t;\alpha^+=.1) - \Delta C^{CS}(t;\alpha^+=10^{-4})$$

Thus, in Fig. 10 the quasi-static load discontinuity is removed from the critical-state response. Note that, in order to calculate ΔC_{dyn}^{CS}, a "quasi-static" critical-state response had to be generated in such a way that the "stop angles," $\alpha(\tau_c-\epsilon)$ and $\alpha(\tau_c+\epsilon)$ matched closely those used at $\alpha^+ = 0.1$. Figure 10 depicts the purely dynamic portion of the critical-state response. As previously noted, the crossing of the critical state is associated with a large transient response.

5.4. Model Prediction

There are two levels of testing of the indicial theoretical prediction. The first level involves reproducing the very maneuver from which the indicial and critical-state responses were determined, prior to the indicial step. The first level of testing examines the feasibility of smoothly blending a finite number of discrete indicial functions to predict the unsteady aerodynamic response in the case where these indicial responses are known exactly. By "known exactly" we mean that there should not be any error or uncertainty in the indicial function due to effects of prior motion history. Such issues are addressed by the second level of testing, which assesses the accuracy of the prediction for *novel*

maneuvers, based only on a finite number of pre-recorded indicial and critical-state responses.

In order to assess the importance of including the critical-state response, we start by presenting results in which functional interpolation error is reduced to a minimum by using all available indicial functions (with the exception, naturally, of those between $\tau_c - \epsilon_1$ and $\tau_c + \epsilon_2$). Functional interpolation error is also reduced further by ensuring that the critical-state-response interval, $[\tau_c - \epsilon_1 , \tau_c + \epsilon_2]$ be "sufficiently large" to encompass the region of rapid change. This region is typically located after the crossing of the critical state. Thus, the interval $[\tau_c - \epsilon_1 , \tau_c + \epsilon_2]$ is asymmetric, with $\epsilon_2 > \epsilon_1 > 0$. For example, near perfect agreement between data and prediction is shown in Fig. 11, using $\epsilon_1 = 2\Delta t$ and $\epsilon_2 = 6\Delta t$. For reference, the "quasi-static" stall curve (obtained using a very small pitch rate, $\alpha^+ = 0.0001$) is also shown in the figure. Excellent agreement is also observed for the prediction of the pitching moment build-up, $\Delta C_m(t)$, shown in Fig. 12.

The predictions of Figs. 11 and 12 correspond to a constant pitch maneuver with $\alpha^+ = 0.04$. Figure 13 compares data and indicial theoretical predictions of the sectional lift build-up, ΔC_l, at $\alpha^+ = 0.02$, $\alpha^+ = 0.04$, and $\alpha^+ = 0.06$. An overall prediction accuracy on the order of one percent is observed at $\alpha^+ = 0.02$ and $\alpha^+ = 0.04$. At $\alpha^+ = 0.06$, the prediction accuracy is not as good (approximately seven percent, on average). There are at least two possible causes for the decreased accuracy at larger rates. The first one is related to the sampling (recall that the validity and accuracy of the globally constructed response depends on the indicial response being the leading order term in some Taylor series expansion valid about the local α; this condition may not be adequately satisfied at the higher pitch rates, since Δt is fixed). The second possible cause of decreased accuracy may be the presence of a second critical state near $\alpha \approx 55°$.

5.5. Reduction

"Reduction" is defined as the process of determining an equivalent sparse sampling of the indicial function space, while retaining the prediction accuracy of the nonlinear indicial model. The results of the study of Ref. 11 suggest that, given the knowledge of the critical state(s),[2] the nonlinear indicial prediction can be of arbitrarily high accuracy, provided that a sufficient number of indicial responses is available. For example, at a pitch rate of $\alpha^+ = 0.04$, a near perfect prediction is obtained (see Fig. 12), using one indicial function every 0.275° in angle of attack (i.e., a total of over 200 indicial functions for the duration of the maneuver shown in Fig. 12) **!** However, it would be impractical to use such a large number of indicial functions, especially with several state variables.

The accuracy of the indicial theoretical prediction model depends on the accuracy of the indicial functional interpolation scheme. This accuracy, in turn, depends critically on adequate sampling of the indicial function space. If too many indicial functions are required, then the method may not be economical in practice, particularly when one deals with multiple degrees of freedom (not just α, as in the present study).

For the same pitch rate of $\alpha^+ = 0.04$, Fig. 14 shows that it is possible to choose as little as nine indicial responses and maintain a reasonably good predictive accuracy throughout the maneuver. The deterioration of the prediction accuracy is illustrated by comparing the prediction using only nine indicial responses to the prediction using almost 300 indicial responses. Note that, in general, the location (angle of attack) corresponding to these indicial responses needs to be optimized. To this end, it has been shown (Ref. 11) that artificial intelligence-based tools can automate the task of partitioning the indicial function space and "recognize" the presence of critical states.

5.6. Prediction of Novel Maneuvers

The second level of testing of the indicial method involves demonstrating the possibility of predicting the load time history for an arbitrary novel maneuver, i.e., one for which neither the indicial functions nor the critical-state response are known ahead of time.

As a byproduct of the first level of testing for constant pitch rate maneuvers at $\alpha^+ = 0.02$, 0.04 and 0.06, 38 indicial responses and 3 critical-state responses were recorded and stored. Previous research (Ref. 1) based on the application of nonlinear

[2] i.e., both α_{CS} and ΔC^{CS}

indicial theory to the Goman-Khrabrov differential equation model suggests that, at a minimum, a parameterization of the indicial function space using the instantaneous α and $\dot{\alpha}$ ought to be used. There is no assurance *a priori* that such a parameterization is adequate. However it is a logical first step, the implementation of which is described below.

The location of the 38 recorded indicial functions in $(\alpha, \dot{\alpha})$ parameter space is shown in Fig. 15. These 38 indicial functions are referred to as the functional interpolation nodes of the prediction method. To test the method, two novel maneuvers are considered. The first maneuver is a variable pitch rate, cosine-type, ramp from 0 to 60° angle of attack, with a maximum pitch rate $\alpha^{+}_{max} = 0.05$. The second maneuver is a blended double cosine ramp from 0 to 50° angle of attack, with a maximum pitch rate $\alpha^{+}_{max} = 0.045$. Both hypothetical maneuvers are depicted in Fig. 16.

The parameter space representation of these two maneuvers is given in Fig. 17, along with several key indications such as dynamic stall (as measured by the peak lift), and the location of the critical-state-response interval $[\alpha(\tau_c - \epsilon_1), \alpha(\tau_c - \epsilon_2)]$ (denoted CSR in the figure). Also indicated in the figure (dotted lines) are the trajectories corresponding to the prior motion history of each of the interpolation nodes. Both the indicial responses and the critical-state responses are functionally interpolated in $(\alpha, \dot{\alpha})$ parameter space. Thus, the prediction of the load build-up for a novel maneuver is a completely "hands-off" process: it does not require any prior knowledge of the critical-state response associated with that maneuver, nor does it require any knowledge of any of the indicial functions associated with it.

$\therefore$

The resulting indicial theoretical prediction for maneuvers #1 and #2 is shown in Figs. 18 and 19, respectively. The results of Figs. 18 and 19 demonstrate that, as in the study of the Goman-Khrabrov model (Ref. 1), indicial theory, coupled with appropriate multivariate functional interpolation methods, can be used as a high angle-of-attack prediction method. This latest demonstration shows that this is so, even in the case where the crossing of a critical state is encountered. An equally important result is that a two-dimensional parameterization of the indicial function space (in this instance, based on α and $\dot{\alpha}$) appears to be sufficient to characterize the effects of prior motion history on the indicial functions.

6. COMPARISON WITH THE METHOD OF STABILITY DERIVATIVES

In what follows, two distinct applications of the method of aerodynamic stability derivatives to the neural network system are presented. The first application is a so-called constant coefficient approach. In the second application, the coefficients are obtained from a table look-up and from actual calculations.

6.1. Constant Coefficient Aerodynamic Derivatives

For comparison purposes, a simple stability-derivative approach was implemented and tested. A priori, it is assumed that (as a minimum) the sectional loads for the rectangular wing can be modeled according to terms in angle of attack and pitch which are linear, except for an alpha-dependence of the pitch damping derivative, and for a quadratic term in alpha, i.e.:

$$C_l = C_{l_0} + C_{l_\alpha}\alpha + C_{l_{\alpha^2}}\alpha^2 + C_{l_q}(\alpha)\,q + C_{l_{\dot{\alpha}}}(\alpha)\,\dot{\alpha}$$
$$C_m = C_{m_0} + C_{m_\alpha}\alpha + C_{m_{\alpha^2}}\alpha^2 + C_{m_q}(\alpha)\,q + C_{m_{\dot{\alpha}}}(\alpha)\,\dot{\alpha}$$

using standard notation. The inclusion of the quadratic term is the lowest order nonlinearity in α. Since the configuration is symmetric, it is understood that the coefficients of even powers of α, such as $C_{l_{\alpha^2}}$, $C_{m_{\alpha^2}}$, must change sign for negative α.

Also, since the motion of the wing is forced around the 1/4 chord point, the pitch rate q and plunge rate $\dot{\alpha}$ are really not independent. We write, therefore, for simplicity

$$\Delta C_l = C_{l_\alpha}\alpha + C_{l_{\alpha^2}}\alpha^2 + C_{l_q}(\alpha)\,q$$
$$\Delta C_m = C_{m_\alpha}\alpha + C_{m_{\alpha^2}}\alpha^2 + C_{m_q}(\alpha)\,q$$

where the pitch rate q is the nondimensional pitch rate (referred to in this study as α^{+}), and it is understood that the wing experiences simultaneously a streamwise-varying plunge. The constant coefficients[3] C_{l_α}, C_{m_α}, $C_{l_{\alpha^2}}$, $C_{m_{\alpha^2}}$ were determined from the neural network data using standard identification

[3] $C_{l_\alpha} = 5.22$ $C_{m_\alpha} = -0.144$ $C_{l_{\alpha^2}} = -4.46$ $C_{m_{\alpha^2}} = 1.136$

techniques. The tabulated parameters $C_{l_q}(\alpha)$, $C_{m_q}(\alpha)$ were determined by the method described in Section 6.2.

Figures 20 and 21 (for ΔC_l, and ΔC_m, respectively) each display three load build-up curves: the data from the neural network (solid line), the nonlinear indicial theoretical prediction (short dashes), and the prediction obtained using the above implementation of the stability-derivative approach (long dashes). Except for the correction provided by the alpha-dependent pitch damping derivative terms, the "constant coefficient" stability-derivative predictions in Figs. 20 and 21 are little more than a test of the validity of the quadratic assumption for ΔC_l, ΔC_m and do not show any evidence of critical state nor, of course, of dynamic stall.

6.2. Table Look-Up with Dynamic Derivatives

An alternative to the "constant coefficient" stability-derivative prediction is to use "table look-up" for static aerodynamics $C_l(\alpha)$, $C_m(\alpha)$, augmented with alpha-dependent pitch damping derivatives:

$$\begin{aligned} C_l(\alpha;q) &= C_l(\alpha;0) + C_{l_q}(\alpha)\, q \\ C_m(\alpha;q) &= C_m(\alpha;0) + C_{m_q}(\alpha)\, q \end{aligned} \qquad (4)$$

The terms $C_l(\alpha;0)$ and $C_m(\alpha;0)$ are the quasi-static lift and moment curves. The terms $C_{l_q}(\alpha)$ and $C_{m_q}(\alpha)$ are the pitch damping derivatives. They were determined from Eq. (4) applied at two pitch rates ($\alpha^+ = 0.2$ and $\alpha^+ = 10^{-4}$) by eliminating $C_l(\alpha;0)$ and $C_m(\alpha;0)$. Having determined the pitch damping derivatives as a function of α, Eq. (4) was used to predict the constant pitch rate maneuver at $\alpha^+ = 0.04$, using $q = 0.04$. The resulting predictions are shown in Figs. 22 and 23. Neither the "constant coefficient" nor "table look-up" implementations of the method of stability derivatives can correctly predict dynamic stall (whether α_S, ΔC_l^S, or ΔC_m^S). In contrast, nonlinear indicial theory accurately predicts the stall angle as well as the load build-ups from 0° to 60°.

7. CONCLUSIONS

A nonlinear indicial prediction model was developed to predict unsteady aerodynamic responses. The model is based on nonlinear indicial response theory and on functional interpolation of parameterized responses. The nonlinear indicial prediction method was applied to a model problem consisting of an artificial neural network (Ref. 2) which was trained to reproduce the detailed aerodynamic characteristics of a pitching wing undergoing dynamic stall. The validation of the method involved recording a finite number of indicial and critical-state responses which were subsequently used to construct the flow response to arbitrary schedules of $\alpha(t)$.

The indicial method is found to be significantly more accurate than aerodynamic derivatives-based methods, which are not appropriate for true unsteady maneuvers, particularly when critical states are crossed. The present results suggest that indicial theory, coupled with appropriate multivariate functional interpolation methods, could be used as a high angle-of-attack prediction method. These results support the initial conclusions of Ref. 1, even in the case where the crossing of a critical state is encountered, namely, that efficient parameterization of the indicial and critical-state function space appears achievable using only local information, such as the instantaneous angle of attack and pitch rate.

ACKNOWLEDGMENT

This work was supported by Wright Laboratory under Phase I SBIR Contract F33615-95-C-3603. The author wishes to thank Capt. Deborah S. Grismer and Mr. Jerry E. Jenkins for their valuable contributions during this project. The author also wishes to thank Dr. Wil Faller for providing the neural network used in this study.

REFERENCES

1. Reisenthel, P. H.: Development of a Nonlinear Indicial Model For Maneuvering Fighter Aircraft, AIAA Paper No. 96-0896, January 1996.
2. Faller, W. E. and Schreck, S. J.: Unsteady Fluid Mechanics Applications of Neural Networks, AIAA Paper No. 95-0529, January 1995.
3. Nixon, D.: Alternative Methods for Modeling Unsteady Transonic Flows, *Unsteady Transonic Aerodynamics*, Vol. 120 of Progress in Astronautics and Aeronautics, Ed. by D. Nixon, AIAA, 1989.
4. Lesieutre, D. J., Reisenthel, P. H., and Dillenius, M. F. E.: A Practical Approach for Calculating Aerodynamic Indicial Functions with a Navier-Stokes Solver, AIAA Paper No. 94-0059,

January 1994.

5. Reisenthel, P. H., Lesieutre, D. J., and Nixon, D.: Prediction of Aeroelastic Effects for Sea-Skimming Missiles with Flow Separation, AIAA Paper No. 91-1052, April 1991.
6. Reisenthel, P. H. and Nixon, D.: Application of Indicial Theory to the Prediction of Unsteady Separation, AIAA Paper No. 91-1742, June 1991.
7. Reisenthel, P. H.: Towards a Semi-Analytic Tool for the Prediction of Dynamic Stall, AIAA Paper No. 94-0537, 1994.
8. Tobak, M., Chapman, G. T., and Schiff, L. B.: Mathematical Modeling of the Aerodynamic Characteristics in Flight Dynamics, NASA TM 85880, 1984.
9. Tobak, M. and Chapman, G. T.: Nonlinear Problems in Flight Dynamics Involving Aerodynamic Bifurcations, NASA TM 86706, 1985.
10. Jenkins, J. E. and Myatt, J. H.: Modeling Nonlinear Aerodynamic Loads for Aircraft Stability and Control Analysis, AGARD Report 789, pp. 13/1-13/10, February 1993.
11. Reisenthel, P. H.: Novel Application of Nonlinear Indicial Theory For Simulation and Design of Maneuvering Fighter Aircraft, WL-TR-95-3094, December 1995.
12. Faller, W. E., Schreck, S. J., and Luttges, M. W.: Real-Time Prediction and Control of Three-Dimensional Unsteady Separated Flow Fields Using Neural Networks, AIAA Paper No. 94-0532.
13. Faller, W. E., Schreck, S. J., Helin, H. E., and Luttges, M. V.: Real-Time Prediction of Three-Dimensional Dynamic Reattachment Using Neural Networks, AIAA Paper No. 94-2337.

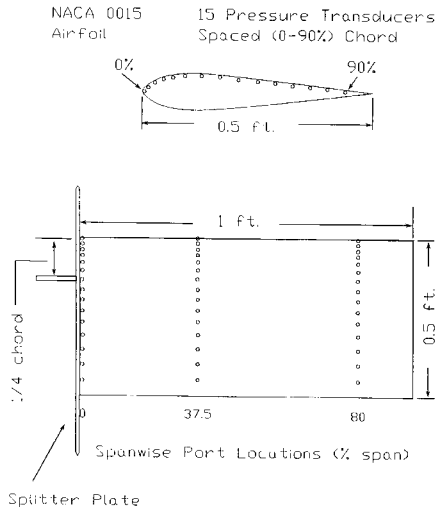

Fig. 1. Schematic Illustrating the Rectangular Wing Used to Train the Artificial Neural Network. (from Ref. 13).

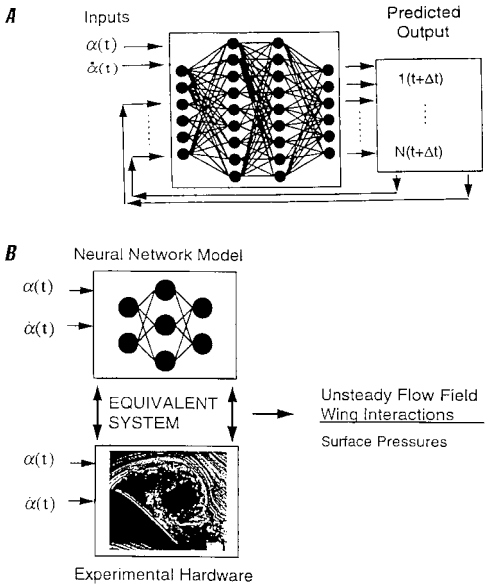

Fig. 2. (A) Schematic of the Neural Network Architecture. (B) The Operational Neural Network Following Training (Fixed Weights). (Adapted from Ref. 2, with permission).

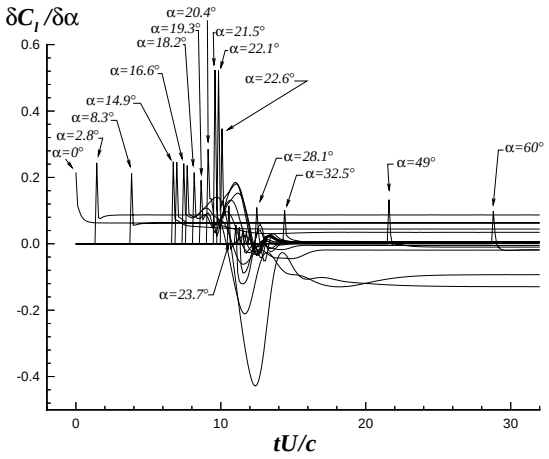

Fig. 3. Plot of 23 Indicial Responses Illustrating the Wide Variations in the Character of the Responses with Angle of Attack, $\alpha^+=0.04$.

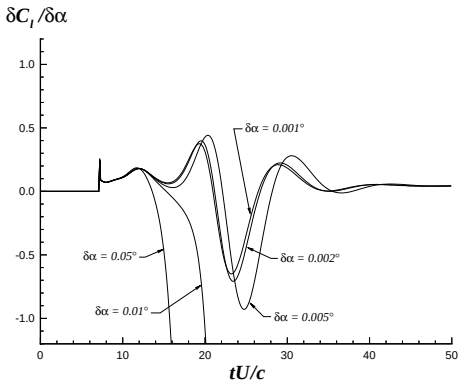

Fig. 4. Convergence of Lift Coefficient Indicial Response with Step Size at $t^*=7.32$ ($\alpha\approx16.3°$), $\alpha^+=0.04$.

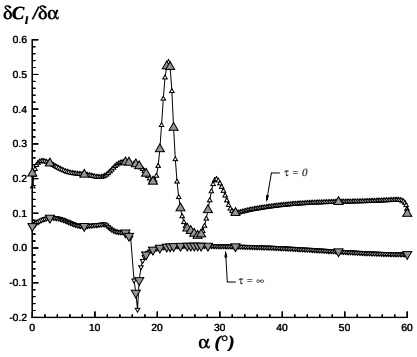

Fig. 5. Variation of Initial and Time-Asymptotic Values of the Lift Indicial Response as a Function of Angle of Attack, $\alpha^+=0.04$. (Large triangles indicate the location of the 23 indicial responses shown in Fig. 3).

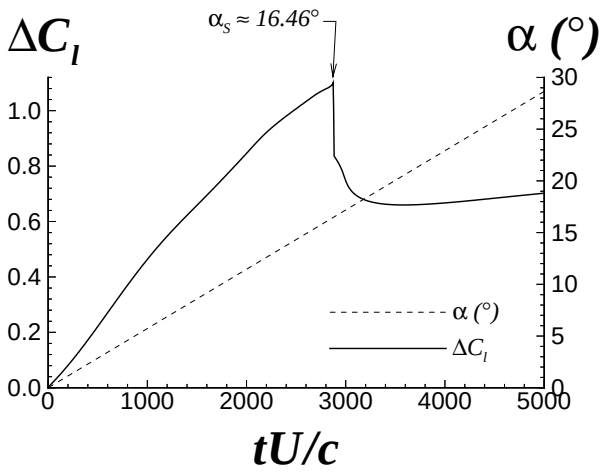

Fig. 6. Quasi-Static Lift Curve. (Obtained using $\alpha^+=10^{-4}$).

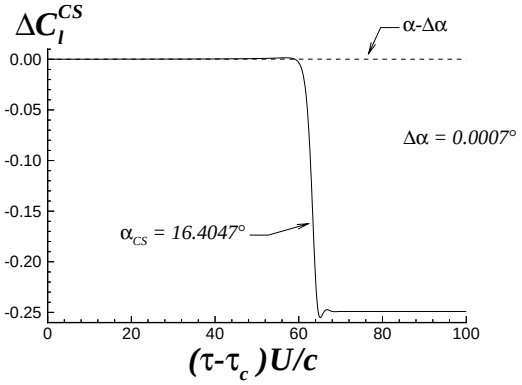

Fig. 7. Variation in the Measured Windowed Response as a Function of CSR Interval Location, $\alpha^+=10^{-4}$.

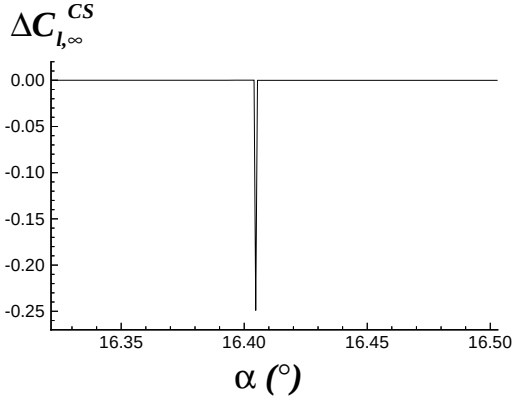

Fig. 8. Variation of the Time-Asymptotic CSR as a Function of the Window Interval Location Near α_{CS}, $\alpha^+=10^{-4}$.

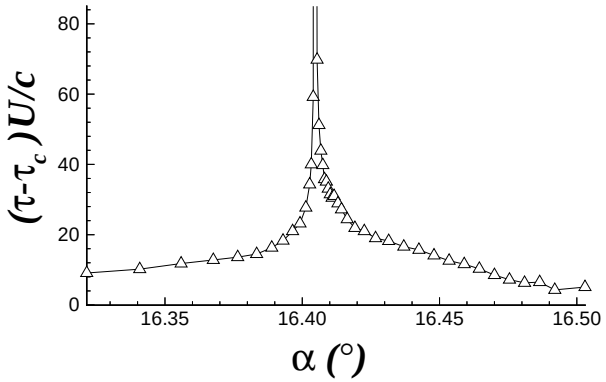

Fig. 9. Variation of the CSR Transient Duration as a Function of the Window Interval Location Near α_{CS}, $\alpha^+=10^{-4}$.

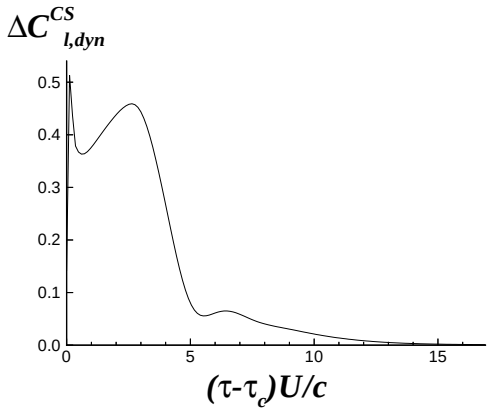

Fig. 10. Dynamic Component of the Critical-state Response for $\alpha^+=0.1$.

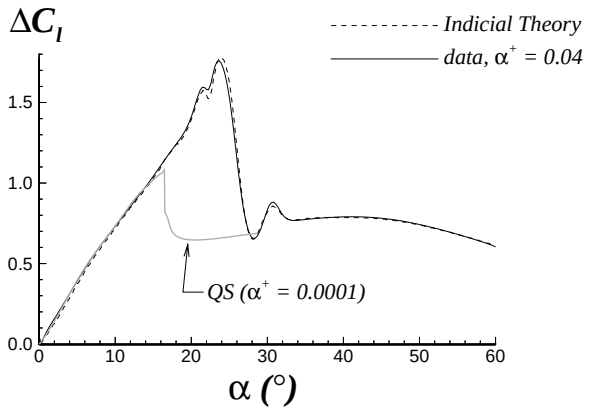

Fig. 11. Lift Indicial Theoretical Prediction Versus Data, $\alpha^+=0.04$. (The quasi-static lift curve is indicated for reference).

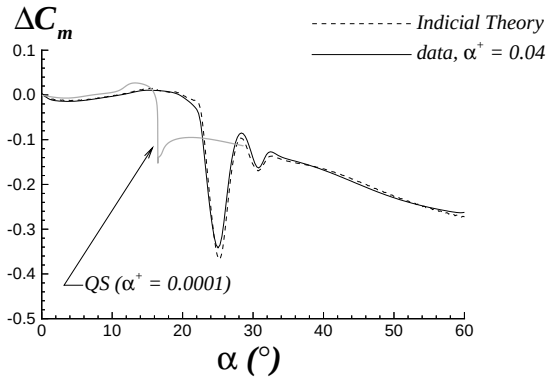

Fig. 12. Pitching Moment Indicial Theoretical Prediction Versus Data, $\alpha^+=0.04$. (The quasi-static moment curve is indicated for reference).

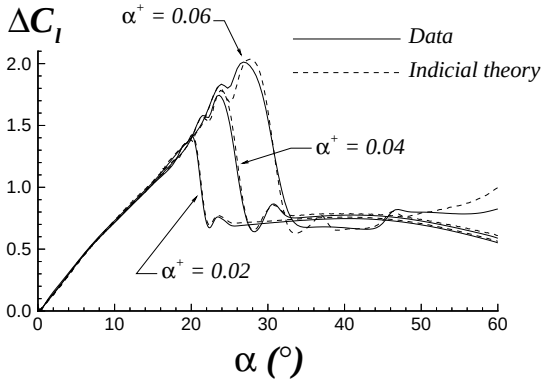

Fig. 13. Indicial Theoretical Prediction Versus Data at Various Pitch Rates.

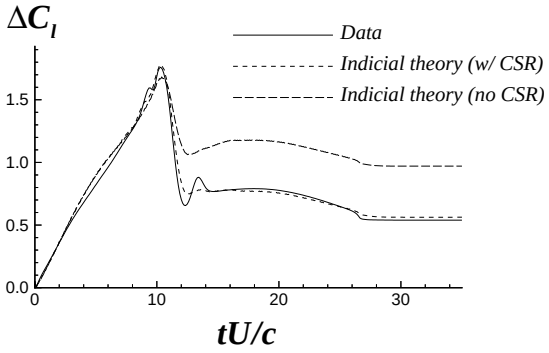

Fig. 14. Indicial Theoretical Prediction at $\alpha^+=0.04$ Using 9 Indicial Response, With and Without Explicitly Accounting For the Crossing of a Critical State.

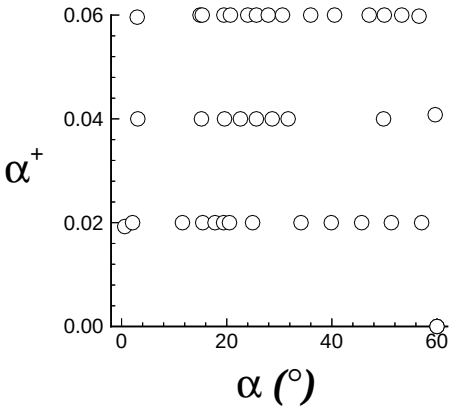

Fig. 15. Parameter Space Representation of the 38 Functional Interpolation Nodes.

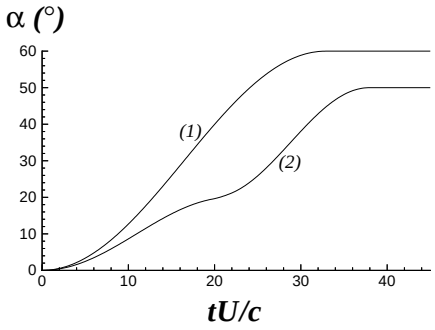

Fig. 16. Angle of Attack Time History of Two Novel Maneuvers.

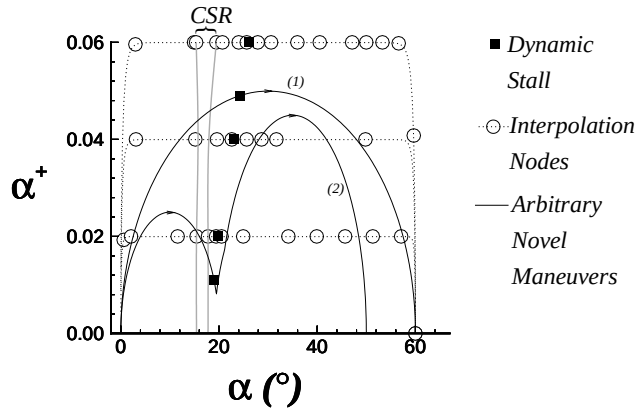

Fig. 17. Parameter Space Representation of Two Novel Maneuvers Illustrating Their Trajectory in Relation With the Location of the Functional Interpolation Nodes. (The grey vertical lines marked "CSR" delimit the critical-state response interval, $[\tau_c - \epsilon_1, \tau_c + \epsilon_2]$).

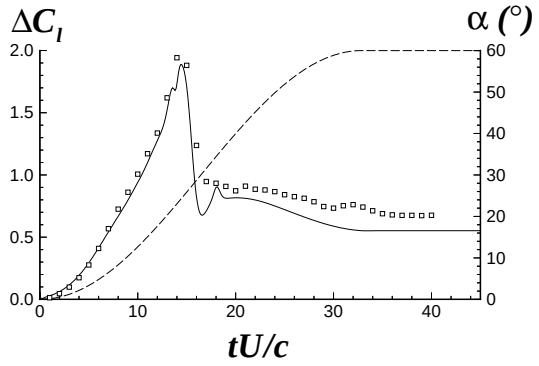

Fig. 18. Indicial Theoretical Prediction for Novel Maneuver #1. (Solid line: data; symbols: indicial theoretical prediction; dashed line: angle of attack history).

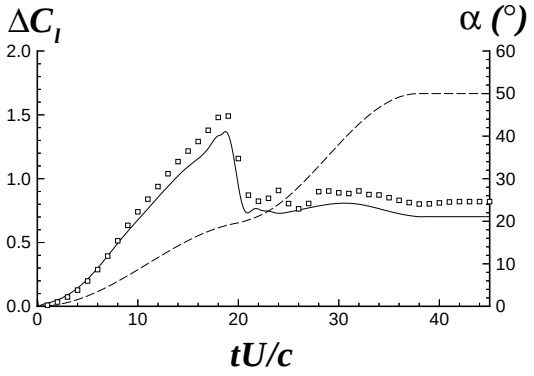

Fig. 19. Indicial Theoretical Prediction for Novel Maneuver #2. (Solid line: data; symbols: indicial theoretical prediction; dashed line: angle of attack history).

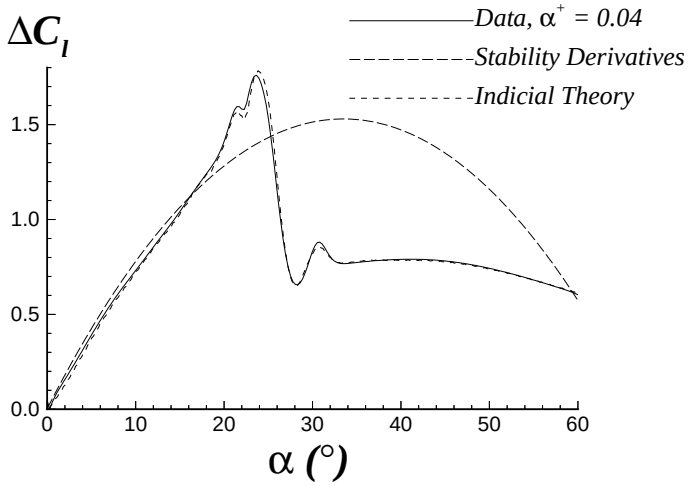

Fig. 20. Comparison of Indicial Theoretical Prediction for Lift Versus the Method of Stability Derivatives, Using Constant Coefficients.

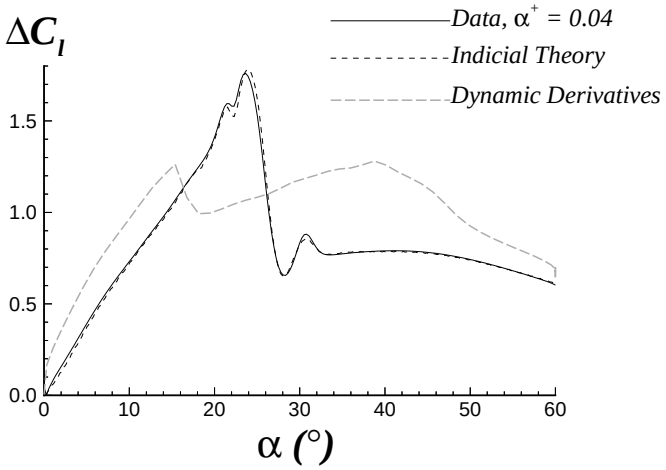

Fig. 22. Comparison of Indicial Theoretical Prediction for Lift Versus the Method of Dynamic Stability Derivatives, Using α-Dependent Pitch Damping Derivative.

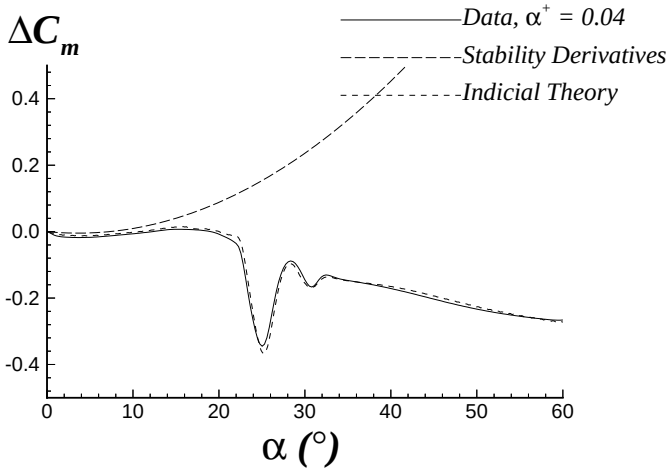

Fig. 21. Comparison of Indicial Theoretical Prediction for Pitching Moment Versus the Method of Stability Derivatives, Using Constant Coefficients.

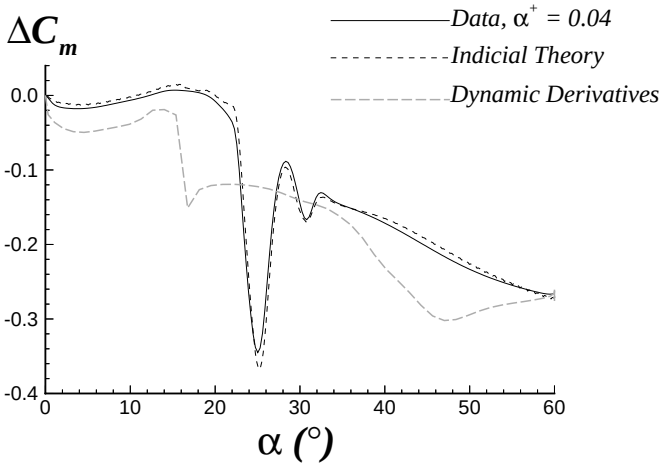

Fig. 23. Comparison of Indicial Theoretical Prediction for Pitching Moment Versus the Method of Dynamic Stability Derivatives, Using α-Dependent Pitch Damping Derivative.